Bioactive Materials 25 (2023) 333–346

Contents lists available at ScienceDirect

Bioactive Materials

journal homepage: www.keaipublishing.com/en/journals/bioactive-materials

A "T.E.S.T." hydrogel bioadhesive assisted by corneal cross-linking for in situ sutureless corneal repair

Meiyan Li [a,b,d,1], Ruoyan Wei [a,b,d,1], Chang Liu [a,b,d,1], Haowei Fang [f], Weiming Yang [a,b,d,e], Yunzhe Wang [a,b,d], Yiyong Xian [a,b,d], Kunxi Zhang [f,**], Yong He [c,***], Xingtao Zhou [a,b,d,*]

[a] Department of Ophthalmology, EYE & ENT Hospital of Fudan University Shanghai, China
[b] NHC Key Laboratory of Myopia (Fudan University), Shanghai, China
[c] State Key Laboratory of Fluid Power and Mechatronic Systems, School of Mechanical Engineering, Zhejiang University, Hangzhou, China
[d] Shanghai Research Center of Ophthalmology and Optometry, Shanghai, China
[e] Department of Ophthalmology, Children's Hospital of Fudan University, National Children's Medical Center, Shanghai, China
[f] Department of Polymer Materials, School of Materials Science and Engineering, Shanghai University, Shanghai, China

ARTICLE INFO

Keywords:
Tough hydrogel
Bioadhesives
Corneal patch
CXL
Sutureless repair

ABSTRACT

Corneal transplantation is an effective clinical treatment for corneal diseases, which, however, is limited by donor corneas. It is of great clinical value to develop bioadhesive corneal patches with functions of "Transparency" and "Epithelium & Stroma generation", as well as "Sutureless" and "Toughness". To simultaneously meet the "T.E.S.T." requirements, a light-curable hydrogel is designed based on methacryloylated gelatin (GelMA), Pluronic F127 diacrylate (F127DA) & Aldehyded Pluronic F127 (AF127) co-assembled bi-functional micelles and collagen type I (COL I), combined with clinically applied corneal cross-linking (CXL) technology for repairing damaged cornea. The patch formed after 5 min of ultraviolet irradiation possesses transparent, highly tough, and strongly bio-adhesive performance. Multiple cross-linking makes the patch withstand deformation near 600% and exhibit a burst pressure larger than 400 mmHg, significantly higher than normal intraocular pressure (10–21 mmHg). Besides, the slower degradation than GelMA-F127DA&AF127 hydrogel without COL I makes hydrogel patch stable on stromal beds *in vivo*, supporting the regrowth of corneal epithelium and stroma. The hydrogel patch can replace deep corneal stromal defects and well bio-integrate into the corneal tissue in rabbit models within 4 weeks, showing great potential in surgeries for keratoconus and other corneal diseases by combining with CXL.

1. Introduction

Corneal diseases are among the most common causes of visual damage and blindness globally [1]. The most effective treatment for advanced corneal diseases is corneal transplantation, which, however, is available for only 5% of these patients. In addition to the donor shortage and the high expense of surgery, allografts may carry an inherent risk of immune rejection and infection [2,3]. Besides, the procedure requires advanced surgical skills and the use of sutures is associated with complications such as suture erosions, infiltrates at the suture sites, infectious keratitis, loose sutures with imminent wound dehiscence, and wound dehiscence after suture removal [4–6]. Developing corneal

Abbreviations: GelMA, Methacryloylated Gelatin; F127DA, Pluronic F127 diacrylate; AF127, Aldehyded Pluronic F127; COL I, Collagen Type I; CXL, Corneal Cross-linking; ECM, Extracellular Matrix; IOP, Intraocular Pressure; UV, Ultraviolet; RF, Riboflavin-5-phosphate; ROS, Reactive Oxygen Species; PBS, Phosphate-buffered Saline; TEM, Transmission Electron Microscopy; DLS, Dynamic Light Scattering; DMEM, Dulbecco's Modified Eagle's Medium; FBS, Fetal Bovine Serum; CCK-8, Cell Counting Kit-8; AS-OCT, Anterior Segment Optical Coherence Tomography; H&E, Hematoxylin and Eosin; IHC, Immunohistochemistry; α-SMA, Alpha Smooth Muscle Actin; SD, Standard Deviation.

Peer review under responsibility of KeAi Communications Co., Ltd.

* Corresponding author. Department of Ophthalmology, EYE & ENT Hospital of Fudan University Shanghai, China.
** Corresponding author.
*** Corresponding author.
E-mail addresses: zhangkunxi@shu.edu.cn (K. Zhang), yongqin@zju.edu.cn (Y. He), doctzhouxingtao@163.com (X. Zhou).
[1] These authors contributed equally to this work.

https://doi.org/10.1016/j.bioactmat.2023.02.006
Received 23 October 2022; Received in revised form 16 January 2023; Accepted 7 February 2023

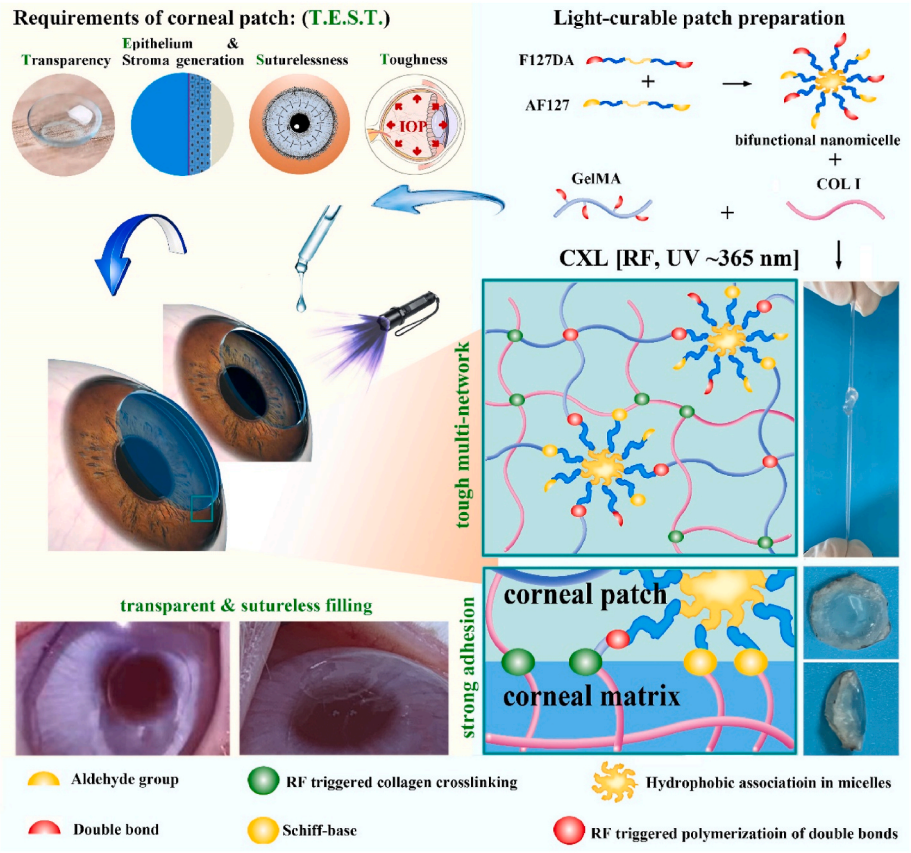

Scheme 1. Fabrication and application, as well as networks illustration of light-curable adhesive corneal hydrogel patch.

substitute for sutureless implantation, which structurally and functionally mimic the native cornea, is a potential approach to promote endogenous regeneration of the cornea [4,7,8].

According to the uniqueness of corneal tissue, functions including a well-integration to adjacent tissues, protection and light transmission need to be focused on in the design of corneal substitutes [9]. On one hand, given the risk associated with surgical sutures, substitutes that can adhere directly and tightly to cornea without sutures are attractive for clinical operation [10,11]. On the other hand, substitutes should support corneal repair and regeneration and mechanically match with cornea matrix to exhibit protection. Specifically, substitutes should support the extracellular matrix (ECM) regeneration of stroma, as well as the development of a functional corneal epithelium, to protect the intraocular contents from pathogenic invasion. At the same time, substitutes should be robust to withstand intraocular pressure (IOP) and other damages [12]. Besides, substitutes should achieve a high degree of transparency (>90%) to mimic the basic optical function of the cornea [12]. Thus, four key performances of corneal substitutes are proposed, including “Transparency”, “Epithelium & Stroma generation”, “Sutureless” and “Toughness”, which was abbreviated to “T.E.S.T.” in the present study.

Hydrogels have received extensive attention as corneal substitutes for their advanced potential in transparency and bionics, such as high water content, biocompatibility, and permeability [13]. Specially, hydrogels fabricated from collagen and its derivatives mimic the ECM composition of the corneal stroma, possessing well-performed biocompatibility and bioactivity [13]. As a polydisperse protein produced from the irreversible hydrolysis of collagen fibrils, gelatin is an excellent component for stimulating cellular attachment and growth [14]. The gelatin-based hydrogels with various cross-linking strategies have been developed for corneal repair [12,14,15]. Among them, gelatin methacryloyl (GelMA) is most widely used as a corneal substitute due to its controlled cross-linking under light irradiation, which is convenient for the preparation of in-situ curable hydrogels that can precisely fill the corneal damage with different shapes [16]. Of note, in-situ light-curable GelMA-based hydrogels are reported to show certain anchoring ability on corneal tissue [17,18]. However, considering the moisture of the ocular surface, as well as the frequent external stimulation to hydrogel caused by eye movements and blinks, the adhesion between GelMA and cornea tissue is inadequate, which is attributed to the weak interfacial adhesion and the low cohesion caused by excessive water absorption and swelling [14]. Corneal tissue adhesion of GelMA-based hydrogels needs to be further improved.

Simultaneous improving the interface adhesion between GelMA hydrogel and corneal tissue and the cohesion of hydrogel is a direct way to improve tissue adhesion of GelMA-based bioadhesives. Currently, two approaches have been practiced in the literature. On one hand, functional groups including aldehyde group [19], pyrocatechol functional group [20], etc. can endow hydrogels with tissue adhesion properties, which have been used in corneal hydrogels. On the other hand, macromolecules, such as dextran-derivatives, silk fibroin-derivatives, and alginate-derivatives, were reported to be combined with GelMA for preparing bioadhesive with improved interface adhesion and cohesion [21,22]. Although there are methods available to improve the strength and tissue adhesion of hydrogels, not all of them are applicable to corneal tissue because of the sacrifice of light transmittance and the adverse impact on their biological properties during the enhancement process. GelMA-based strong biological adhesive for cornea has not been well developed. It is a great challenge to improve both interface adhesion and cohesion of GelMA-based hydrogel while ensuring biocompatibility and transparency.

In addition, ultraviolet (UV) light and visible light are commonly used for the development of in-situ curable GelMA adhesives/hydrogels in ophthalmology [15,17]. Although UV light might pose potential

threats to the eye compared to visible lights, it played a unique role in clinical application. Corneal cross-linking (CXL), an FDA-approved procedure for slowing the progression of keratoconus, uses UV-A light and riboflavin-5-phosphate (RF) to induce cross-linking of collagen [23]. Reactive oxygen species (ROS) generated during RF photosensitization mediates the production of new covalent bonds between collagen molecules, leading to an increase in biomechanical strength and stiffness of the corneal stroma [24,25]. Of note, RF has a high absorption effect on UV (~370 nm) rays, preventing most UV light from passing through the cornea. The Young's modulus of collagen-based hydrogel has been shown to significantly increase after UV irradiation mediated by RF [26–28]. However, as the collagen derivative, GelMA-based hydrogel cross-linking used in cornea repair is mostly based on type I photoinitiators such as Irgacure-2959, UV curing of GelMA based on CXL technology has not been well-developed but worth studying.

Thus, to develop an enhanced bioadhesive GelMA-based hydrogel substitute that can be combined with CXL to match the requirement of "T.E.S.T.", the present study introduced collagen type I (COL I) without any modification, and Pluronic F127 diacrylate (F127DA) & Aldehyded Pluronic F127 (AF127) co-assembled nano-micelles into GelMA (Scheme 1). The presence of co-assembled micelle significantly restricted the swelling of hydrogel and endowed hydrogel with toughness. COL I formed a network triggered by CXL to enhance modulus of hydrogel and to extend the degradation duration. The aldehyde groups in micelle, the linkage between COL I and corneal ECM triggered by CXL, and the light-curable in-situ-formed networks worked together to endow the hydrogel with excellent tissue adhesive ability. After component optimization to ensure transparency, corneal tissue adhesion of hydrogel was evaluated both *in vitro* in a porcine cornea and *in vivo* in a lamellar keratoplasty rabbit model. *In vivo* repair and replacement of deep corneal defects was further evaluated in a rabbit model. Of note, it is worth noting that both the CXL and the components of hydrogel are approved by the FDA for clinical use, making this hydrogel system have a clear prospect of transformation and application.

2. Materials and methods

2.1. Materials

Pluronic F127 (F127) was purchased from Sigma-Aldrich. Acryloyl chloride, p-Toluenesulfonyl Chloride, 4-hydroxybenzaldehyde, methacrylic anhydride, potassium carbonate, triethylamine, collagen type I (COL I), L-arginine and riboflavin-5-phosphate (RF) were purchased from China National Pharmaceutical Group Corporation. Gelatin was purchased from EFL.

2.2. Synthesis of GelMA

Gelatin was added to phosphate buffer medium and stirred at 50 °C until completely dissolved. Then methacrylic anhydride was added for reaction for 3 h. The mixed solution was diluted with phosphate-buffered saline (PBS) to stop the reaction, followed by dialysis for 7 d to completely remove the low molecular weight with potential cytotoxicity impurities. After lyophilization, GelMA power was yielded. FT-IR (NicoletiS10, Thermofischer, Germany) and ^{1}H NMR (AVANCE 500MHZ, Bruck, Switzerland) were used to characterize the synthesized GelMA.

2.3. Synthesis of F127DA and AF127

F127 was added into the round bottom flask. Then, dichloromethane was added to the flask and fully stirred until F127 was completely dissolved. Triethylamine was added as an acid binding agent, and acryloyl chloride was slowly added. After the reaction was in ice water bath for 1 h, the reaction was continued at 25 °C for 24 h. After the reaction was completed, triethylamine hydrochloride precipitation was filtered first, and the filtrate was washed with saturated Na_2CO_3 aqueous solution. After standing for layering, the dichloromethane layer was taken and washed three times. Then the filtrate was washed with saturated NaCl solution. The dichloromethane layer was taken after standing and layering and washed three times. After the organic phase was dried with anhydrous $MgSO_4$, it was concentrated to a small volume by rotary distillation, precipitated with super-cooled ether, filtered by suction to obtain a white solid, and dried in vacuum for 24 h to obtain F127DA.

F127 was dissolved in dichloromethane, followed by addition of pyridine and p-phenylsulfonyl chloride for reaction at room temperature for 24 h. The mixture was extracted with hydrochloric acid, the organic phase was washed with $NaHCO_3$, recrystallized from tetrahydrofuran/diethyl ether mixed solvent, and dried in vacuo to obtain the intermediate product. The intermediate product was dissolved in N,N-dimethylformamide, with the addition of 4-hydroxybenzaldehyde and potassium carbonate, stirred in the reaction at 80 °C for 72 h, and cooled to room temperature. After adding water, the reaction solution was extracted with dichloromethane. The organic layer was dried with $MgSO_4$, concentrated, and precipitated in cold diethyl ether, filtered and vacuum dried to obtain AF127. FT-IR (NicoletiS10, Thermofischer, Germany) and ^{1}H NMR (AVANCE 500MHZ, Bruck, Switzerland) were used to characterize the synthesized F127DA and AF127.

Table 1
Abbreviations of different groups of hydrogel.

Abbreviations	GelMA	F127DA & AF127	COL I
G8F0	8%	0	0
G0F4	0	4% (F127DA = 2%; AF127 = 2%)	0
G8F4	8%	4% (F127DA = 2%; AF127 = 2%)	0
G8F5	8%	5% (F127DA = 2.5%; AF127 = 2.5%)	0
G10F5	10%	5% (F127DA = 2.5%; AF127 = 2.5%)	0
G12	12%	0	0
G8FA4	8%	4% (F127DA = 4%; AF127 = 0)	0
G8FA2&AF2	8%	4% (F127DA = 2%; AF127 = 2%)	0
G8F4C3	8%	4% (F127DA = 2%; AF127 = 2%)	3%
G8F4C4	8%	4% (F127DA = 2%; AF127 = 2%)	4%

2.4. Preparation of hydrogels with multiple networks

F127DA and AF127 with different ratios and concentrations were dissolved in H_2O and treated with ultrasonic wave for 30 min to yield micelle solutions. Transmission Electron Microscopy (TEM, JEM-200cx, JEOL, Japan) and Dynamic Light Scattering (DLS, ZS90, Marlven, British) were carried out to measure the morphology and size of different micelles. Different concentrations of GelMA and COL I were dissolved in micelle solutions to achieve the precursor solution of hydrogel, followed by adding RF (0.1 w/v%) and L-arginine (0.4 wt ratio to GelMA) [29]. In mold, UV irradiation for as long as 5 min was carried out for photo-crosslinking to achieve hydrogels. The naming abbreviations of different groups of hydrogel in this study were shown in Table 1.

Precursor solution of hydrogels in cuvette (10 mm) and hydrogel sheets (1 cm in length, 1 cm in width, 1 mm thick) were subjected for light transmission test on a spectrophotometrically (SpectraMax M2, Molecular Devices, USA) at 37 °C in the range of 400–800 nm.

2.5. Swelling behavior of hydrogel formed after UV irradiation

Hydrogels formed after UV irradiation were weighted and recorded (M_0), which were immersed in PBS to fully swell. After removing excess water, hydrogels were weighed and recorded (M_1), then the mass swelling ratio (S_m) of the sample was calculated according to the following formula: $S_m = (M_1 - M_0)/M_0 \times 100\%$.

2.6. Mechanical tests

The compressive and tensile tests were performed at room

temperature on an Instron 5943 testing machine. Compression tests were performed on cylindrical samples with a diameter of 8 mm and height of 4 mm at 10% strain per minute and stopped at 80% strain. The compression modulus was calculated by the slope of the linear region on the stress-strain curve. Tensile tests were performed on dumbbell-shaped samples (2 mm × 1.5 mm) with a gauge length of 10 mm at a stretching crosshead speed of 100 mm/min until rupture. The tensile strength was obtained at the breaking point. The toughness was calculated from the area under the stress-strain curve. The tensile modulus was calculated from the slope of the stress-strain curves.

2.7. Burst pressure test

The adhesive property and sealing ability of the hydrogels on porcine cornea were evaluated by a burst pressure test using a handmade device. A perforation with a diameter of 5 mm was created on a rubber tube, one end of which was connected to a syringe and the other end closed. A pressure gauge detection (ALKC420, AILEIKE, China) was connected to this system. A perforation with a diameter of 6.5 mm was created on a porcine cornea (the thickness was ~1 mm), which was filled with hydrogels. Then, the cornea tissue was fixed onto the rubber tube to cover the notch of the rubber tube with medical glue FAL(NOCA + NBCA). Deionized water was continuously flowed into the tube by a syringe pump to induce an intraocular-like pressure until leakage was identified. The leakage could be identified by recording the peak pressure before pressure loss, which was considered the burst pressure.

2.8. Lap shear test

To evaluate the tissue adhesive ability of hydrogel patches, two cornea tissues were fixed onto the glass slide with medical glue FAL (NOCA + NBCA). Hydrogel precursor solutions of 50 μL were dropped onto one cornea. Then the two corneas were closed together and subjected to UV irradiation for 5 min. After gelation, the glued corneas with glass slides were subjected to lap shear test. All tests were carried out at a 50 mm/min shear rate at room temperature. The adhesive strength was defined as the maximum lap shear stress during the test.

2.9. Rheological characterization and viscosity measurement

Rheological Photogelation Kinetics were monitored on a rotational rheometer (Discovery HR20, TA, USA) with a parallel 12 mm plate and a UV light source. The gap was adjusted to 0.4 mm and the shear storage moduli (G') were recorded with a frequency of 0.2 Hz and strain of 5%. After 3 min of recording, the UV light was turned on for irradiation for 6 min while recording continued.

The viscosity of hydrogel precursor solutions was monitored on a rotational rheometer (Discovery HR20, TA, USA) with a parallel 12 mm plate and temperature controller. The gap was set to 0.4 mm and the viscosity (PaS) was recorded with shear rate change from 0.1 to 100 (S^{-1}) at 25 °C and 37 °C.

2.10. Enzymatic degradation of hydrogel patches

To track the degradation of G8F4 hydrogel and G8F4C3 hydrogel, each sample was incubated in 1 ml of bacterial collagenase type I (Sigma, 5 U mL^{-1} in 0.1 M PBS). Each sample was weighted on days 0, 3, 5, 7, 10 and 14. The weight change (%) was calculated.

2.11. Cell cultures and in vitro analysis

Human corneal fibroblasts were purchased from Procell Life Science & Technology Co., Ltd (Wuhan, China), and was cultured in Dulbecco's Modified Eagle's medium (DMEM) with 10% fetal bovine serum (FBS) and 1% penicillin/streptomycin. All cultures were incubated at 37 °C with 5% CO_2.

Before the co-culture, the pre-hydrogels were prepared as described above and filtered through a 0.22 μm filter. Sterile pre-hydrogels were photo-crosslinked in the dishes with ultraviolet for 5 min using a light source (365 nm, 250 W) and washed 3 times with culture medium to get the hydrogel particles (20 μL pre-hydrogels for each particle). For cytotoxicity evaluation of hydrogel, corneal fibroblasts were seeded in the 96-well plates and after 24 h, the particles were transferred in wells (one per well) and the cells were co-cultured with particles. A cell counting kit-8 (CCK-8, Dojindo, Japan) assay was used at 1, 3, 5, and 7 days after co-culture. The particles and culture medium were removed and the wells were washed 3 times with PBS. Then 10 μL of CCK-8 reagent was added into each well and incubated for 90 min. In experimental groups (exp.), cells were co-cultured with different hydrogel particles. In the control group (ctr.), cells were cultured without hydrogels. The absorbance was measured at 450 nm with a microplate reader (Tecan, Switzerland). Cell viability = ($OD_{exp.}$-OD_{black})/($OD_{ctr.}$-OD_{black}) × 100%.

Further, the sterile pre-hydrogel solution containing RF and L-arginine (50 μL for each well) was transferred into 96-well plates and photo-crosslinked with ultraviolet for 5 min using a light source (365 nm, 250 W) and washed 3 times with culture medium. Then, corneal fibroblasts were seeded onto the surfaces of the hydrogel. The cell viability was evaluated qualitatively using a LIVE/DEAD viability/cytotoxicity kit (Beyotime, China) and quantitative with CCK-8 assay after 1, 3, 5, and 7 days. For LIVE/DEAD assay, the hydrogel particles and culture medium were removed and the wells were washed 3 times with PBS. The staining solution containing 1 μM calcein AM and 1 μM propidium iodide was added into the well and the cells were incubated for 30 min at 37 °C in the dark. Live (green stain) and dead (red stain) cells were imaged using an inverted fluorescence microscope (Carl Zeiss Meditec, Germany). CCK-8 assay was performed as mentioned above.

2.12. Animal surgeries

All experiments were conducted in compliance with the ARVO statement for the Use of Animals in Ophthalmology and Vision Research and had ethical approval from Animal Care Committees of Eye and ENT Hospital of Fudan University (IACUC-DWZX-2022-017). Surgery was performed in 12-week-old male New Zealand white rabbits (2.5–3.0 kg) under anesthesia with intravenous injection of Zoletil (13 mg/kg) and xylazine hydrochloride (1.7 mg/kg) and topical application of 0.4% oxybuprocaine hydrochloride ophthalmic solution.

For the lamellar keratoplasty model, a graft was made using a femtosecond laser system (Carl Zeiss Meditec) with a repetition rate of 500 kHz and pulse energy of 230 nJ at a depth of approximately 2/3-3/4 corneal thickness. The graft diameter was set to 6.5 mm. The lamella was removed and prepared for transplantation, the recipient stroma bed was irrigated and the excessive fluid on the corneal surface was wiped dry with a sponge. The pre-hydrogels were then applied to the stroma bed and spread out as a thin film. The donor graft, previously prepared by femtosecond laser with compatible thickness, was fitted into place and the extra pre-hydrogels were squeezed out from the interface and removed with a sponge. The pre-hydrogels were photo-polymerized with UV light (365 nm, 250 W) for 5 min. The 0.5% levofloxacin eye drop and tobramycin/dexamethasone ointment were applied to the eyes three times daily for one week.

For corneal defect healing model, the defect was made using Mel-90 excimer laser (Carl Zeiss Meditec) with a repetition rate of 250 Hz and pulse energy of 1 mJ. The ablation zone was set to 3.0 mm, and the corneal was ablated at a depth of approximately 1/2 corneal thickness (~250 μm). The pre-hydrogels were applied to the defect and photo-polymerized with UV light (365 nm, 250 W) for 5 min. The 0.5% levofloxacin eye drop and tobramycin/dexamethasone ointment were applied to the eyes three times daily for the first week and usage was gradually reduced in the following three weeks.

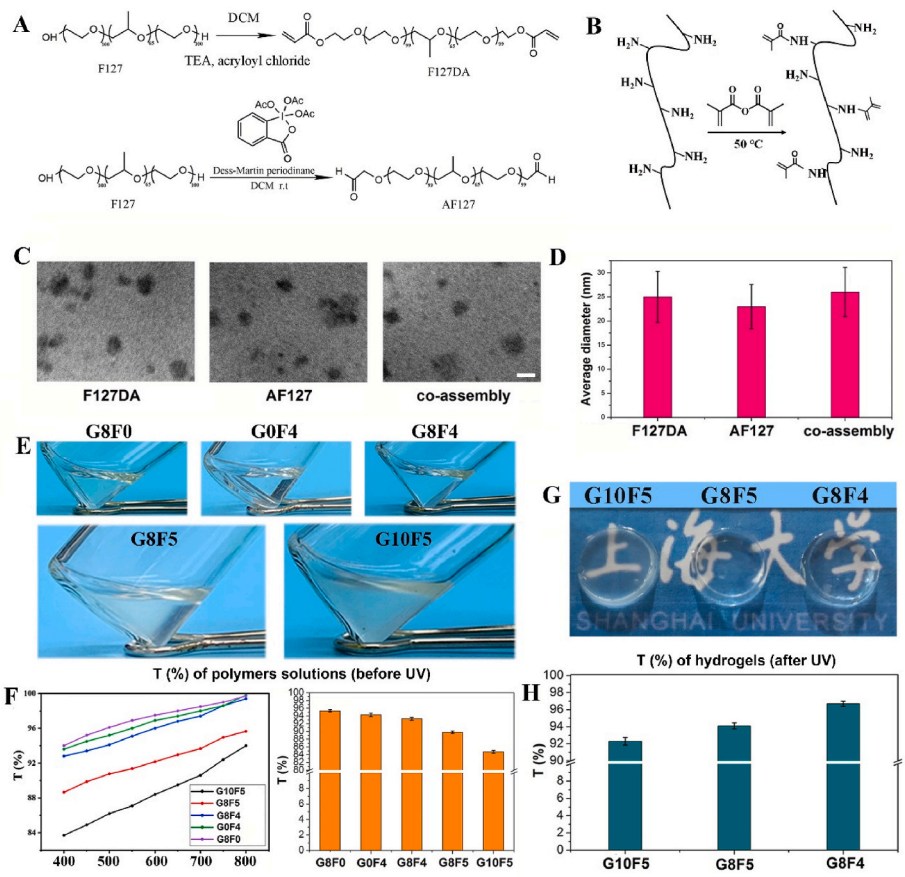

Fig. 1. Synthesis, micelle fabrication, and hydrogel fabrication. **A.** Synthesis of GelMA. **B.** Synthesis of F127DA and AF127. **C.** TEM images of F127DA micelle, AF127 micelle and co-assembled F127DA&AF127 micelle (bar scale: 20 nm, F127DA: AF127 = 1:1). **D.** Average particle size statistics. **E.** General transparency observation of precursor solution of GelMA, micelles and their mixture. **F.** Light transmission over the visible light spectrum, and light transmission at 450 nm. **G.** General transparency observation of hydrogels after UV irradiation. **H.** Light transmission of hydrogels at 450 nm.

2.13. Slit-lamp and anterior segment optical coherence tomography (AS-OCT)

For the lamellar keratoplasty model, eyes were evaluated with a slit lamp (Mediworks, Shanghai, China) and AS-OCT (Optovue, Inc., Freemont, CA) immediately and 7 days after the surgery; while for the corneal defect healing model, eyes were evaluated immediately, 3, 7, 14, and 28 days.

A slit lamp in diffuse illumination and a narrow beam was used to evaluate the corneal transparency. To assess the migration of corneal epithelium over the adhesive, cobalt blue slit lamp photography with fluorescein staining was performed. The line-scan mode in AS-OCT was used to evaluate the depth of the defect and the healing process.

2.14. Histological analysis

Rabbits were euthanized 4 weeks after surgery. The corneal tissue was harvested and fixed in 10% formaldehyde, paraffin-embedded, sectioned and stained with hematoxylin and eosin (H&E) reagent and Masson's trichrome according to the manufacturer's instructions. Immunohistochemistry (IHC) staining was also conducted. After an antigen retrieval method was applied on each section with citrate buffer (PH = 6.0), tissues were incubated with an anti-alpha-smooth muscle actin (α-SMA) primary antibody (GB13044, 1:200; Servicebio, China) overnight at 4 °C and with an HRP-conjugated secondary antibody (GB23301, 1:200; Servicebio) antibody at room temperature for at least 2 h.

2.15. Statistical analysis

All continuous variables are presented as mean ± standard deviation (SD). Student's *t*-test was applied to compare variables between groups. A p-value less than 0.05 was considered statistically significant.

3. Results and discussion

3.1. Preparation of the GelMA/F127DA&AF127 hydrogel

Gelatin and F127 was pre-functionalized to possess double bonds so that the synthesized GelMA and F127DA could undergo photo-crosslinking with the presence of photosensitizers. In addition, to further enhance the bio-adhesion ability of hydrogel, F127 was aldehyde functionalized to achieve AF127. GelMA, F127DA, and AF127 were successfully synthesized according to Fig. 1A and B, and characterized by ^{1}H NMR and FT-IR (Fig. S1). Of note, F127 is a well-studied polymer that can self-assemble into nano-micelle in water [30,31]. Similarly, according to Fig. 1C, F127DA, AF127 and F127DA&AF127 could also self-assemble into nano-micelles in water. Three kinds of micelles were fabricated, including F127DA micelle, AF127 micelle and co-assembled F127DA&AF127 micelle. The different terminal groups and the co-assembly of F127DA&AF127 did not significantly affect the micelle size. DLS tests showed that the three **kinds of** micelles showed a similar average size, which was about 25 nm (Fig. 1D).

Either GelMA or the self-assembled F127DA&AF127-micelles dissolved in PBS showed excellent transparency. The transmittance slightly decreased after the mix of GelMA and the F127DA&AF127-micelles, while still showing high transmittance. For example, the transmittance of G8F4 (concentration of GelMA was 8%, concentration of F127DA&AF127-micelles was 4%, F127DA:AF127 was 1:1) was about 92%. However, with the increase of F127DA&AF127-micelle concentration and the increase of total polymer concentration, transmittance decreased significantly (Fig. 1E and F). Visual opacity was observed. For the treatment of corneal defects, the pre-mixed GelMA and the F127DA&AF127-micelles solution was injected into the defect region,

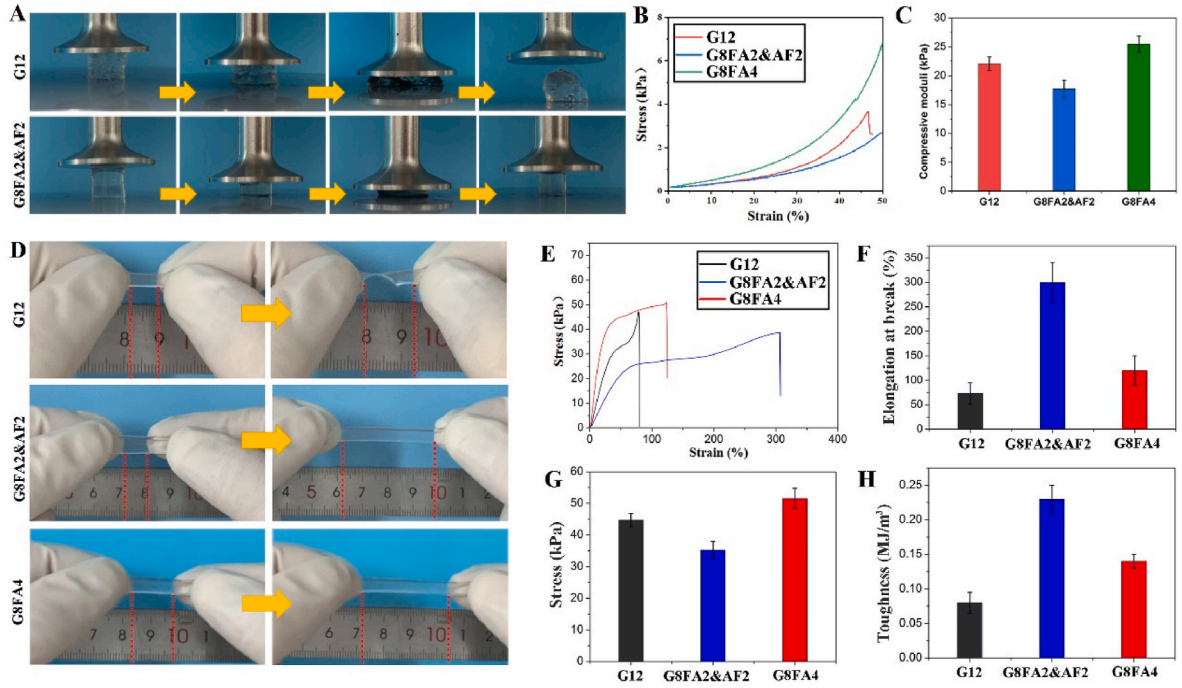

Fig. 2. Compression and tensile tests on hydrogels. **A.** General observation of GelMA hydrogel and GelMA with co-assembled micelles hydrogel under compression. **B.** Stress-stain curves of hydrogels during compression testes. **C.** Compressive moduli of hydrogels. **D.** General observation of GelMA hydrogel, GelMA with co-assembled micelles hydrogel and GelMA with F127DA micelles hydrogel under stretching. **E.** Stress-strain curves of hydrogels during tensile testes. **F.** Elongation at break of hydrogels. **G.** Fracture stress of hydrogels. **H.** Toughness of hydrogels.

followed by a short-term UV irradiation for gelation. Because RF alone could not initiate the photo-crosslinking reaction of the unsaturated double-bonded polymer solution upon UV irradiation. L-arginine which acted as an electron donor in the photo-initiation process, was used as a coinitiator to trigger the unsaturated GelMA and F127DA photo-induced gel formation. Thus, in addition to evaluating the transparency of the polymers solutions, the transparency of the hydrogel formed after UV curing also needed to be evaluated to exclude the possibility of the influence of the UV curing process and related initiators on the transparency.

After UV exposure for 5 min, a solidified hydrogel was achieved, which was immersed in PBS for simulating the tear film in the eyes (Fig. 1G). Because the normal human corneal thickness is less than 1 mm, the present study fabricated hydrogel sheet with a thickness of 1 mm for transmittance detection. As shown in Fig. 1G, hydrogels with higher total polymer concentration showed significant visual opacity after immersing in PBS for 24 h. The transmittance test showed that G8F4 hydrogel sheets with a thickness of 1 mm possessed good transmittance, which was as high as 96% (Fig. 1H). Since transparency is essential for corneal repair, a high degree of transparency (>90%) should be ensured when the hydrogel composition is adjusted [12].

3.2. Mechanical performance of GelMA/F127DA&AF127 (GxFAn&AFm) hydrogel

Improving the toughness of gelatin-based hydrogels was one of the focuses of this study, and also a challenge. Given the swelling of gelatin-based hydrogel, they were usually easily damaged. F127DA and AF127 were triblock copolymers containing two amphiphilic block polymers, which possess self-assembly behavior that is driven by hydrophilic and hydrophobic interactions in an aqueous solution. The hydrophobic block chains form the core while the hydrophilic block chains form the shell of the micelle. Non-covalent interactions in micelles take the responsibility to consume the external loading via its dissociation, making hydrogel robust to withstand large deformation [32–34].

Thus, as shown in Fig. 2A, B, C, the gelled GelMA hydrogel, G12 was easier to be destroyed by compressive force. The stress-strain curve showed that GelMA hydrogel was destroyed when the strain was less than 50%. However, under the same polymer content, the hydrogels, G8FA2&AF2 with the introduction of F127DA(2%)&AF127(2%) micelles subjected to ultimate compression, showed no damage. Hydrogels with either F127DA&AF127 micelles or F127DA micelles could withstand large deformation. The micelles acted as the huge cross-linking units that bound inside gel network. In addition to double bonds on micelle surface that linked to gel network, aldehyde groups on micelle surface could form Schiff-base with GelMA, and hydrophobic chains in core of micelles endowed the hydrogel with excess physical cross-linking units, which contributed most to the improvement of toughness. Hydrogel made from GelMA (8%) and F127DA(2%)&AF127(2%) micelle (G8FA2&AF2) showed lower compressive modulus than hydrogel made from GelMA (8%) and F127DA (4%) micelle (G8FA4), which might be related the reduced number of double bonds in F127DA&AF127 micelle.

Considering the limited deformation of compression test, tensile test was used to evaluate the toughness of hydrogels. As shown in Fig. 2D, GelMA hydrogel, G12 was easy to break under tensile action, while hydrogel G8FA2&AF2 and G8FA4 showed larger deformation. However, according to tensile tests (Fig. 2E,F), F127DA micelles showed a limited effect on the improvement of hydrogel toughness. The breaking elongation of hydrogel G8FA4 was about 120%, while the breaking elongation of hydrogel G8FA2&AF2 was about 300%. Thus, compared with hydrogel G8FA4, hydrogel G8FA2&AF2 exhibited significantly improved toughness. This was related to the decrease of double bond density in co-assembled F127DA&AF127 micelle. For one thing, the decrease in double bond density improved the degree of micelle freedom in hydrogel network. F127DA macromolecules that make up micelles are chemically connected into the hydrogel network, while AF127 macromolecules were freer. Upon loading, the freer macromolecules in micelles were able to move more freely with the sliding and deforming of micelles, delaying the dissociation of micelles. For another, aldehyde

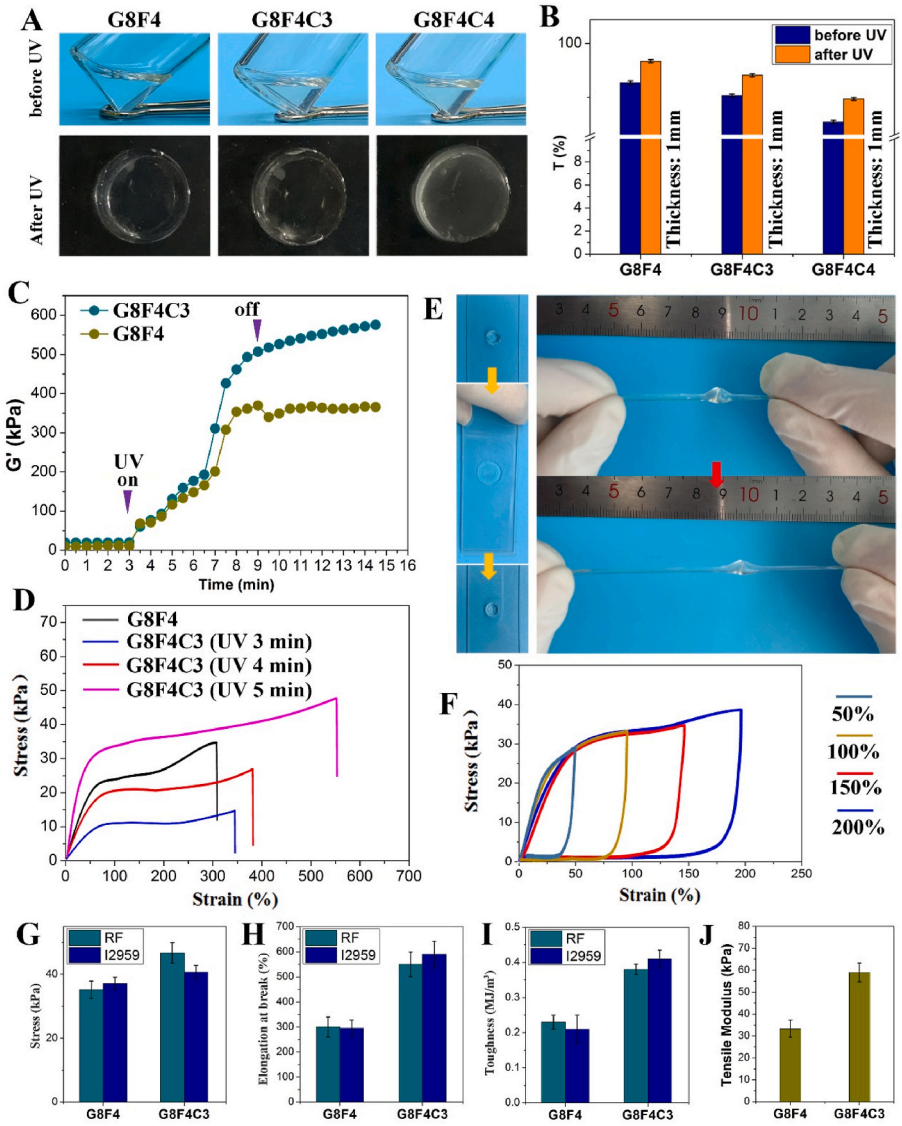

Fig. 3. Effect of COL I on transparency and mechanical performance of hydrogel. **A.** General transparency observation of precursor solutions and gelled hydrogels. **B.** Light transmission of precursor solutions and hydrogels at 450 nm. **C.** G′ of G8F4 and G8F4C3 hydrogels monitored while curing with UV to record the gelatin kinetics of hydrogels. **D.** Stress-strain curves of hydrogels during tensile testes. **E.** General observation of G8F4C3 hydrogel under extreme compression and stretching. **F.** Loading-unloading curves of G8F4C3 hydrogel. **G.** Fracture stress of hydrogels. **H.** Elongation at break of hydrogels. **I.** Toughness of hydrogels. **J.** Tensile moduli of G8F4 and G8F4C3 hydrogels.

group in AF127 might form Schiff-base with amino groups of GelMA, which could act as sacrificial bonds to dissipate stress [35]. Thus, although the tensile modulus of hydrogel G8FA2&AF2 decreased, the toughness was significantly enhanced (Fig. 2G and H). Compared with F127DA micelles, the application of F127DA and AF127 co-assembled micelles in GelMA hydrogel performed better in improvement of hydrogel toughness. The GelMA (8%) with F127DA (2%)&AF127 (2%) co-assembled micelles hydrogel, G8FA2&AF2, which was defined as G8F4 for short, was used for further studies.

3.3. Transparency and mechanical performance of GelMA/F127DA&AF127/COL I (GxFyCz) hydrogel

Based on the above hydrogel toughening strategy, the present study further introduced collagen I (COL I) into the tough hydrogel to compensate for the loss of modulus in G8F4 (G8FA2&AF2), and endow the hydrogel with bionic characteristics because COL I is the main component of the corneal matrix.

Firstly, the transparency of the hydrogel after the introduction of COL I was evaluated. According to Fig. 3A and B, after the addition of COL I, the transparency was slightly reduced either before or after UV irradiation. In addition, the more COL I was added, the lower the transparency of hydrogel was. The introduction of collagen macromolecules had a negative impact on the transparency of hydrogels, which might be related to the poor solubility of collagen compared with gelatin. However, hydrogel sheet with 3% COL I (G8F4C3) and a thickness of 1 mm still possessed sufficient transparency (>90%) (Fig. 3B), which was used for further studies.

On the premise of ensuring good transparency, the study further evaluated the effect of COL I introduction and CXL technology on the mechanical performance of hydrogels. Unlike the negative effect of COL I addition on transparency, the COL I addition showed a positive effect on hydrogel mechanical properties. For one thing, the photo-gelation kinetics were monitored. According to the recorded shear storage moduli (G′) in Fig. 3C, both G8F4 hydrogel and G8F4C3 hydrogel underwent rapid photo-gelation during the first minute of curing with UV light. In addition, with the extension of exposure time, the G′ of G8F4 hydrogel and G8F4C3 hydrogel increased significantly. After 5 min irradiation, the G′ of G8F4 hydrogel stopped increasing and remained relatively stable. While the G' of G8F4C3 hydrogel kept increasing, but the increase was smaller.

For another, as shown in Fig. 3D, both the elongation at break and the tensile strength of G8F4C3 hydrogels increased with the increase of irradiation time. G8F4C3 hydrogel after 5 min UV irradiation showed significantly improved elongation at break and tensile strength when compared with G8F4 hydrogel. The elongation at break was over 500%,

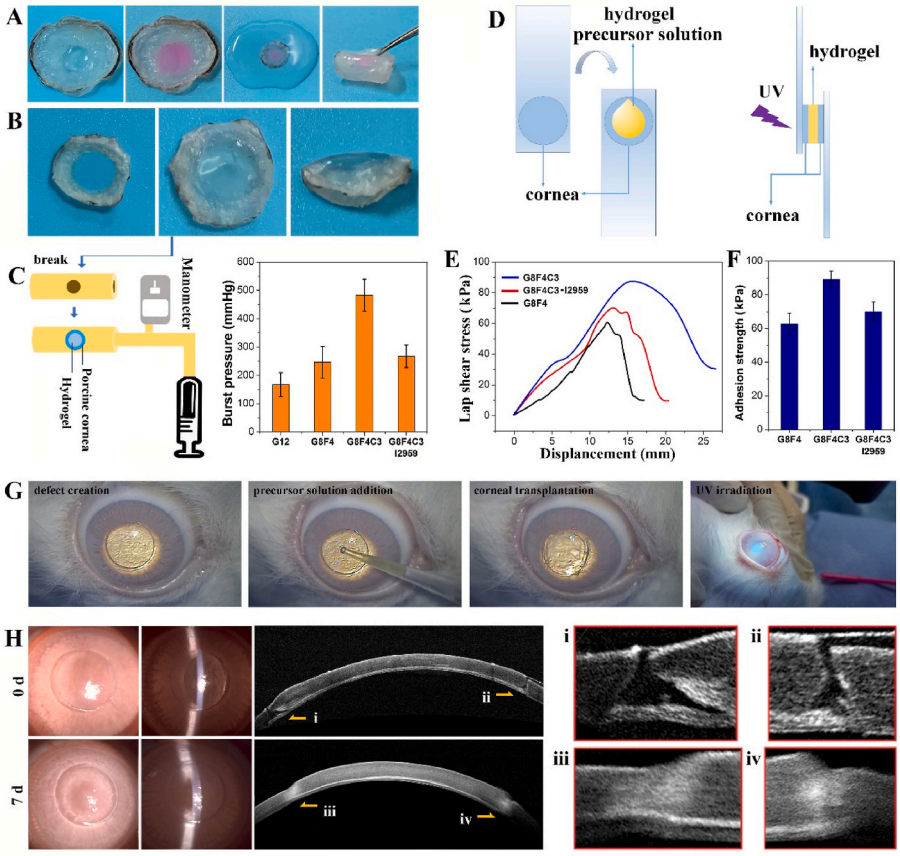

Fig. 4. Adhesive ability of hydrogel G8F4C3. **A.** General observation of hydrogel G8F4C3 adhered to *in vitro* porcine cornea defect. **B.** Hydrogel G8F4C3 adhered to penetrating porcine cornea defect for burst test. **C.** Burst test device and burst pressure. **D.** Scheme of lap shear test. **E.** Lap shear adhesion curve of hydrogels to cornea. **F.** Adhesion strength of hydrogels. **G.** Operation process of corneal transplantation *in vivo* to evaluate the adhesive ability of hydrogel G8F4C3. **H.** Slit lamp photographs and Anterior segment optical coherence tomography (AS-OCT) images after sutureless lamellar keratoplasty using G8F4C3 hydrogel at 0 d and 7 d.

significantly higher than that of G8F4 hydrogel. According to compression test, the compressive modulus of G8F4C3 was significantly higher than that of G8F4 (Fig. S2). G8F4C3 hydrogel was also robust and could be extremely compressed without being damaged. In addition, after knotting, the hydrogel strips show extremely high tensile deformation under tensile action (Fig. 3E). Besides, according to the loading-unloading cyclic tensile tests in Fig. 3F, the hysteresis loops illustrated the physical cross-linking effect in hydrogel. The repeatability of the loading-unloading curves at different maximum strains revealed that the hydrogel possessed good deformation recovery ability.

The mechanism of mechanical enhancement was further studied. Theoretically, according to our design based on CXL, the UV photo-initiation system used RF as photo-initiator and L-arginine as a coinitiator could not only trigger the unsaturated GelMA and F127DA photo-induced gel formation, reactive oxygen species (ROS) produced by RF but also could cross-link the COL I in hydrogel, forming an additional network, which contributed to the mechanical enhancement of hydrogel. To confirm the formation of cross-linked COL I network, hydrogels gelation triggered by another photo-initiator, I2959 was fabricated and underwent tensile tests. As shown in Fig. 3G,H,I, tensile strength and elongation at break, as well as toughness were all enhanced after COL I addition in both RF group and I2959 group. While G8F4C3 hydrogel triggered by RF showed significantly higher tensile strength than G8F4C3 hydrogel triggered by I2959, indicating the formation of cross-linked COL I network when using RF as photo-initiator. Besides, according to Fig. 3J, the tensile test showed that the tensile modulus of G8F4C3 hydrogel was near 60 kPa, higher than that of G8F4 hydrogel. Thus, mechanical enhancement was related to the addition of COL I and its cross-linking triggered by ROS produced by RF after UV irradiation.

On one hand, CXL technology using RF is internationally recognized as the main treatment to prevent and delay the progression of keratoconus [23]. Accordingly, ROS generated during RF photosensitization mediates the production of new covalent bonds between collagen molecules, leading to an increase in biomechanical strength and stiffness of the corneal stroma [24,25]. The Young's modulus of collagen-based hydrogel has been reported to significantly increase after UV irradiation mediated by RF [26–28]. The application of RF in the cornea is clinically verified to be safe and effective. On the other hand, GelMA-based hydrogels reported in the literature for corneal repair are mostly UV or visible light-triggered cross-linking [15,17]. These hydrogels had different moduli due to different concentrations and different photo-crosslinking methods, but they all showed the same problem that they were easy to be damaged. Tensile test was rarely seen in the research of GelMA-based corneal hydrogels. In the compression test, the destruction deformation of GelMA-based corneal hydrogel was less than 60% [17,27], which indicated that the ability of GelMA-based hydrogel to resist destruction was poor. Even if other components such as silk fibroin were introduced into GelMA-based hydrogel, the destruction deformation of the composite hydrogel could only be increased to about 90% [21]. However, in the compression test of this study, the hydrogel could not be damaged. In the tensile test, the exercise elongation of hydrogel was as high as 600%. This confirmed that the present hydrogel, G8F4C3 was more robust.

3.4. Cornea adhesion performance of GelMA/F127DA&AF127/COL I hydrogel

Hydrogels used for sutureless repair of corneal injuries require sufficient adhesion with adjacent corneal tissues to withstand high IOP and avoid detachment. Thus, cornea adhesion performance of G8F4C3 hydrogels was evaluated. As shown in Fig. 4A, hydrogel G8F4C3 could adhere tightly to the porcine cornea *in vitro*. Even after immersion in water for 24 h, followed by bending and other operations, it still adhered tightly to the cornea without shedding. To further quantitatively

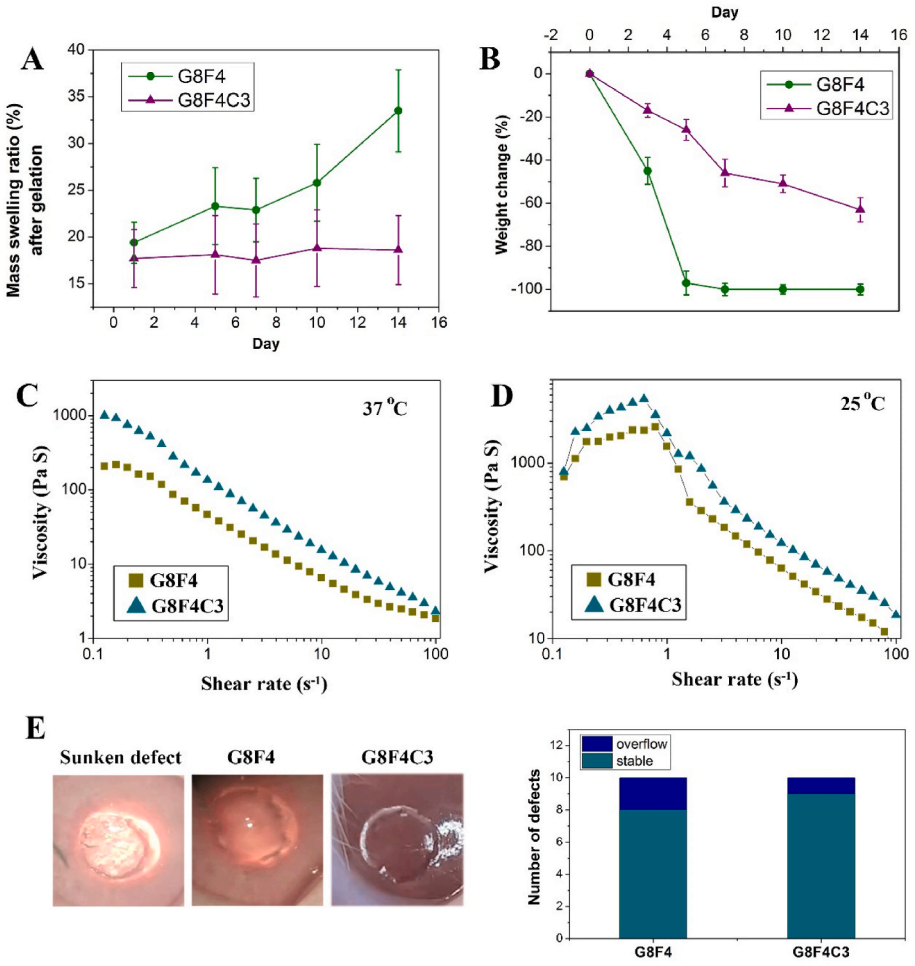

Fig. 5. Swelling, degradation and viscosity of corneal hydrogels. **A.** Mass swelling ratio during incubation in PBS. **B.** Changes in weight of hydrogels incubated with collagenase. **C,D.** Rheological characterization of viscosity of hydrogel precursor solutions with shear rate change at 37 °C and 25 °C. **E.** Representative photos and statistics showing the effect of gravity on the behavior of hydrogel precursor solutions while applied on the defect area during operations.

characterized the adhesion between hydrogel and corneal tissue, a penetrating defect was created on the porcine cornea, and the precursor solution of hydrogel G8F4C3 was filled into the defect and underwent UV irradiation (Fig. 4B). Then, the circular cornea carrying adhered hydrogel after immersion in water for 24 h was fixed onto the damaged part of rubber pipe for a burst pressure test (Fig. 4C). G8F4 and G8F4C3 showed significantly higher burst pressure than G12 because G12 showed lower adhesive ability and was more easily destroyed. In addition, G8F4C3 showed improved burst pressure when compared with G8F4. The burst pressure was larger than 400 mmHg. Of note, G8F4C3 hydrogel that gelled with I2959 showed similar burst pressure with G8F4 hydrogel, significantly lower than G8F4C3 hydrogel that gelled with RF, indicating that the presence of AF127 and COL I in hydrogel not only contributed to the enhanced mechanical performance but also promoted the tissue adhesive property of hydrogel. The lap shear test was also consistent with burst pressure test. G8F4 precursor solution and G8F4C3 precursor solution were dropped into two pieces of porcine cornea, followed by UV irradiation for lap shear test (Fig. 4D). As shown in Fig. 4E and F, all the fractures occurred at the bond between the gel and the cornea. The hydrogels themselves were not damaged. G8F4C3 hydrogel showed higher adhesion strength than G8F4 hydrogel and G8F4C3 hydrogel that gelled with I2959. Both the burst pressure test and the lap shear test illustrated that the G8F4C3 gelled with RF showed the highest cornea adhesion.

Compared with the tissue adhesion of the corneal hydrogels in the literature including GelMA-based hydrogels, the hydrogel prepared in this study showed superior corneal adhesion. According to I.A. Khalil [18], the visible light-curable GelMA hydrogels on a 6 mm rabbit cornea incision showed a maximum burst pressure lower than 20 kPa (150 mmHg), while the present G8F4C3 gelled with RF on a porcine cornea perforation with a diameter of 6.5 mm showed a burst pressure higher than 400 mmHg. Accordingly, light-curable hydrogels, including GelMA-based hydrogels showed effective tissue adhesion ability during in-situ suture-free corneal repair [36,37]. In addition to light-curable hydrogel, the present study introduced aldehyde groups in hydrogel, which has been widely used to promote the tissue adhesion performance of hydrogels [38,39]. More importantly, the presence of COL I could also bond to the cornea matrix after photo-curing with the presence of RF, which had a great contribution to the corneal adhesion of hydrogel. At the same time, the good tissue adhesion of hydrogel is not only related to its ability to combine with the tissue interface, but also related to the mechanical properties of the hydrogel itself. Thus, the enhancement of hydrogel toughness also contributed to the improvement of its corneal adhesion.

The tissue adhesive property was further evaluated on a sutureless corneal transplantation model *in vivo* (Fig. 4G). Fig. 4H showed corneal preservation immediately and 7 days after the operation. According to observation using slit-lamp microscopy and AS-OCT, the corneal graft was firmly attached to the corneal bed. The gap between the graft and the corneal bed immediately after the operation disappeared after 7 days, confirming that the graft and the recipient's cornea achieved effective tissue fusion. At 7 d transplantation, we used a cotton swab to

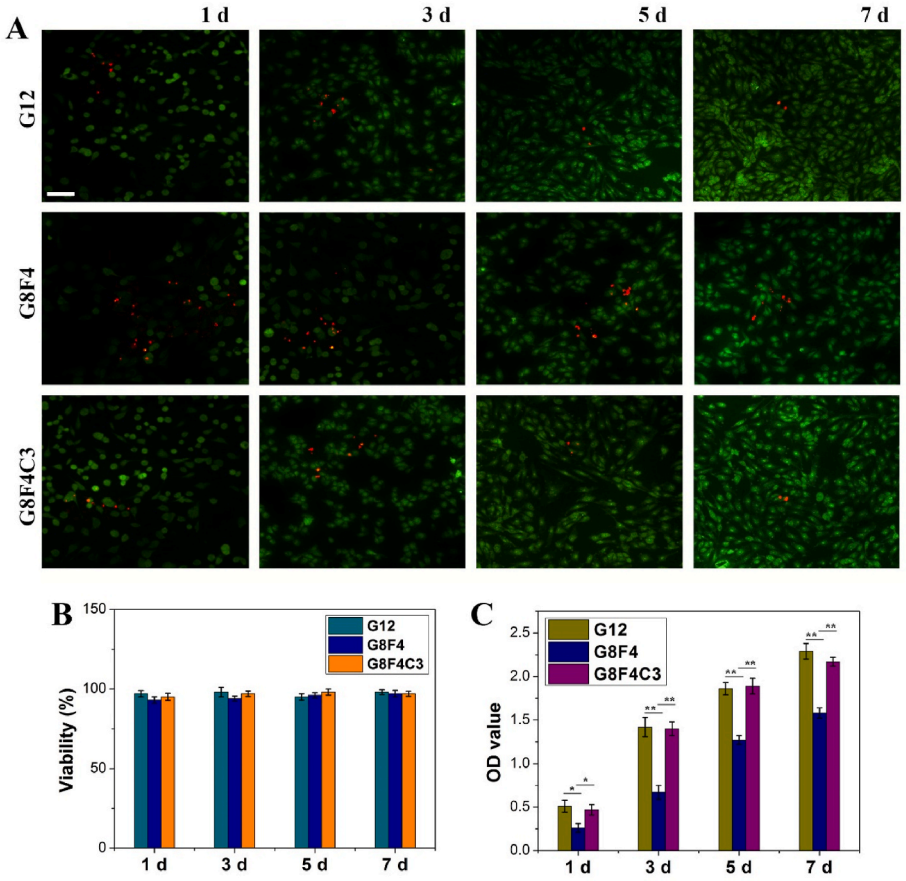

Fig. 6. *In vitro* cytocompatibility of hydrogels. **A.** Live/dead staining of corneal fibroblasts cultured on the surface of G12, G8F4, and G8F4C3 hydrogels (Bar scale: 50 μm). **B.** Cellular viability. C. Corneal fibroblasts proliferated on hydrogels after 1, 3, 5, and 7 days. (*p < 0.05, **p < 0.01).

move the transplanted cornea, the video showed that the corneal graft was firmly attached to the ocular surface, and did not fall off under the pulling force (Supporting **Information, Video**). Thus, based on the *in vitro* and *in vivo* adhesion evaluation, the G8F4C3 associated with CXL was a qualified corneal adhesive and could potentially be used for corneal transplantation.

Supplementary video related to this article can be found at doi:10.1016/j.bioactmat.2023.02.006

3.5. Swelling, degradation, and viscosity of GelMA/F127DA&AF127/COL I hydrogel

Besides the mechanical performance and bioadhesion ability of G8F4C3 hydrogel, the dimensional stability and degradability of the filling gel are also important for long-term corneal injury repair. Thus, the swelling behavior and degradation behavior of G8F4 hydrogel and G8F4C3 hydrogel were monitored. As shown in Fig. 5A, both the G8F4 hydrogel and G8F4C3 hydrogel after UV-triggered gelation showed low further swelling when immersing in PBS, which was lower than 20%. However, further monitoring of continuous immersion in PBS for 14 days showed that the swelling degree of G8F4 hydrogel continued to increase, while the swelling degree of G8F4C3 hydrogel did not change significantly. This result indicated that G8F4C3 hydrogel possessed better dimensional stability during cornea repair. This anti-swelling ability guaranteed the stability of hydrogel size after implantation.

Besides, dimensional stability was also closely related to degradation. Too fast a degradation rate would lead to poor dimensional stability. According to Fig. 5B, G8F4 hydrogel degraded quickly, showing a sharp degradation at 5 days in PBS with collagenase. However, due to the addition of cross-linked COL I network, the degradation of G8F4C3 was significantly delayed, leaving nearly 40% undegraded hydrogel at 14 d. The delayed degradation ensured the hydrogel adhesion, as well as sufficient space for epithelium and stroma regeneration during the corneal repair.

At last, considering that clinically used glues usually show low cohesion on the corneal surface, which leads to the spreading of products on the surface to the unwanted areas after application and before cross-linking, the present tested the viscosity of the hydrogel precursor solutions. Because a low cohesion (very liquid) will make the hydrogel precursor solutions easily spread over the field to undesired areas before cross-linking, while too viscous performance (very high cohesion) will make the hydrogel precursor solutions not adequately spread to provide coverage of the targeted area [37]. As shown in Fig. 5C and D, both G8F4 hydrogel precursor solution and G8F4C3 hydrogel precursor solution exhibited shear-thinning at 37 °C, while showed shear-thickening followed by shear-thinning by increasing in the shear rate at 25 °C. Thus, the G8F4 hydrogel precursor solution and G8F4C3 hydrogel precursor solution showed potential for injection after pre-heating. Besides, the viscosity of G8F4C3 hydrogel precursor solution was higher than G8F4 hydrogel precursor solution at 37 °C and 25 °C. According to intraoperative statistics, in G8F4C3 hydrogel treated group, 9 out of 10 defects had no hydrogel overflow problem, and in G8F4 hydrogel treated group, 8 out of 10 defects had no hydrogel overflow problem. In most cases, the hydrogel precursor solutions dropped into the damaged area of the cornea and stayed in the defect area to complete the subsequent light curing (Fig. 5E).

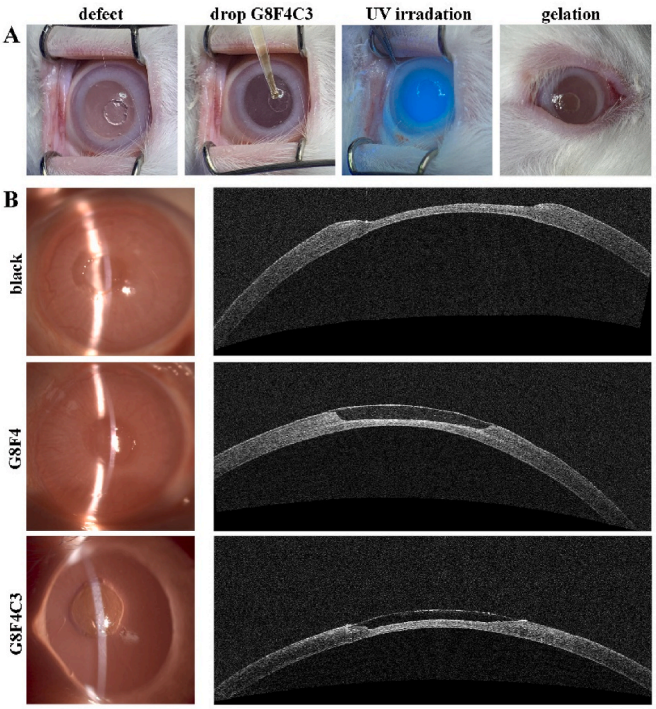

Fig. 7. *In vivo* implantation of the hydrogels into rabbit corneal defects. **A.** Operation process of *in vivo* implantation of hydrogel. **B.** Representative slit lamp images (left) and AS-OCT images (right) after defect creation without treatment and after hydrogel treatments using G8F4 and G8F4C3.

3.6. *In vitro cytocompatibility of GelMA/F127DA&AF127/COL I hydrogel*

To verify the cytocompatibility of hydrogels and the procedure, after gelation with the same operation during *in vivo* application, corneal fibroblasts were seeded onto hydrogel G12, G8F4, and G8F4C3 for *in vitro* cell culture. As shown in Fig. 6A, live/dead staining showed that cells could adhere to the hydrogel surfaces. All hydrogels had no significant cytotoxicity. CCK8 test of co-culture of corneal fibroblasts and hydrogels showed cell viability was higher than 95% (Fig. 6B). In addition, cells that adhered to different hydrogels showed different adhered numbers (Fig. 6A,C). The presence of F127DA&AF127 micelles showed a negative effect on cell attachment. However, the addition of COL I could make up for the adverse effect of F127DA&AF127 micelles on cell adhesion. Cells cultured on hydrogel G8F4C3 kept proliferation during the following *in vitro* culture. The evaluation results of *in vitro* cytocompatibility not only confirmed the potential of GelMA and COL I based hydrogel in supporting epithelium generation, but also confirmed the safety of using RF and L-arginine.

In general, hydrogel G8F4C3 showed minimized swelling, well-performed toughness, and corneal adhesion capability, as well as guaranteed biocompatibility to support cell adhesion, viability, and proliferation. Therefore, hydrogel G8F4C3 was subjected to the following *in vivo* evaluation for corneal defect repair.

3.7. *Repair of deep corneal defects in rabbit eyes*

A rabbit corneal defect model was established with 3.0 mm in diameter and ~250 μm in depth, which was a deeper corneal defect when compared with most literature reports [20,36]. The precursor solutions of G8F4 and G8F4C3 were dropped into the lesion with the same volume as the defect. Five min later, they were exposed to UV irradiation for 5 min to achieve hydrogels in-situ. After gelation, both G8F4 and G8F4C3 adhered well to the stromal beds, exhibiting smooth surfaces. There were no obvious adverse reactions in the rabbit eyes post-surgery. AS-OCT characterization showed that the filled hydrogels exhibited different optical reflectivity from the surrounding corneal stroma (Fig. 7A and B).

After hydrogel implantation, the corneal defects were monitored. For one thing, re-epithelialization could be observed in all groups according to fluorescein staining observation via slit-lamp microscopy in Figs. 8A and 9A, B. The epithelial defect area stained with green fluorescence progressively decreased. Compared with the black group that had no treatment, G8F4 and G8F4C3 hydrogels treated groups showed significantly faster re-epithelialization and the epithelial defects disappeared within 14 days. According to previous reports, the epithelium could be repaired within 7 days after surgery when applying GelMA-based corneal hydrogels [15]. However, the epithelium generation in the present study seemed to be delayed. This might be related to the depth of the corneal defect. The depth used in literature was usually 1/3 of the corneal thickness, while the depth of the defect in this study was 1/2 of the corneal thickness (~250 μm). We speculated that deeper corneal injury might lead to a more intense corneal reaction and slower epithelium reconstruction. The result indicated that G8F4C3 could realize the function of "Epithelium generation".

After 4 weeks post-implantation, corneal defects treated with G8F4 and G8F4C3 hydrogels were relatively transparent and smooth. Images from slit-lamp and AS-OCT photographs showed that the corneal defects

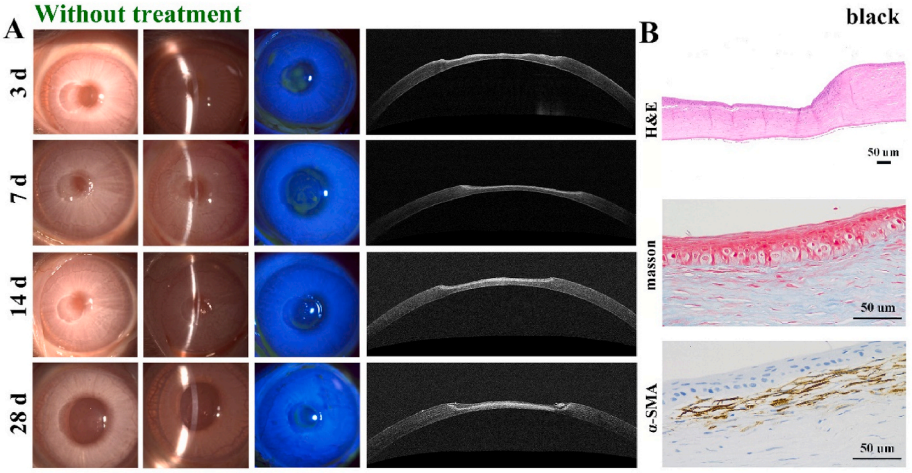

Fig. 8. Postoperative observation of the corneal defects without treatment. **A.** Representative slit-lamp images and AS-OCT images in black group without treatment at 3, 7, 14, and 28 days. **B.** H&E, Masson and α-SMA immunohistochemical staining of regenerated tissue in black group (Bar scale: 50 μm).

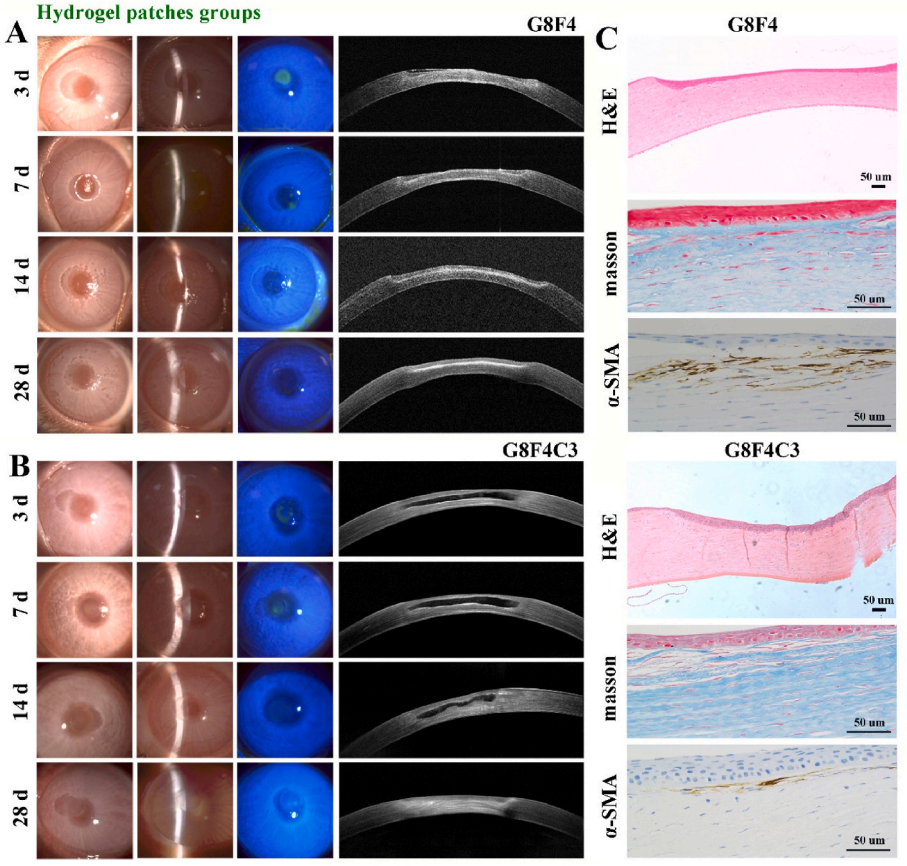

Fig. 9. Postoperative observation of the corneal defects with hydrogels treatment. **A.** Representative slit lamp images and AS-OCT images in G8F4 hydrogel treated group at 3, 7, 14 and 28 days. **B.** Representative slit lamp images and AS-OCT images in G8F4C3 hydrogel treated group at 3, 7, 14 and 28 days. **C.** H&E, Masson and α-SMA immunohistochemical staining of regenerated tissue in G8F4 hydrogel treated group and G8F4C3 hydrogel treated group (Bar scale: 50 μm).

filled with hydrogel G8F4C3 exhibited a thickness closer to the native cornea and a better curvature. While significant concave defects were observed in the black group and G8F4 hydrogel treated group. The poor healing in the black group indicated that the deep corneal defect was difficult to self-repair. Besides, defect regions of all groups showed whitish color. Mild corneal opacity was observed in the AS-OCT photographs, reminding us that a longer period of steroid eye drops may be required to inhibit fibrosis.

Of note, because the optical reflectivity of implanted hydrogels was different from the native cornea, the degradation of hydrogels could be observed via AS-OCT images. In G8F4 treated group (Fig. 9A), hydrogel could be observed at 3 d post-implantation. However, after 7 days, no hydrogels were found in all samples, indicating fast degradation of G8F4 hydrogel. Due to the fast degradation, stromal cells failed to enter the gel to form corneal tissue without the spatial support of hydrogel. Different from G8F4 treated group, G8F4C3 hydrogel showed significantly slower and gradual degradation within 4 weeks. According to Fig. 9B, the hydrogel region was observed to reduce significantly at 14 days post-implantation. During hydrogel degradation, the corneal matrix formed to keep a similar thickness. As shown in Fig. S3, the total thickness of corneas in G8F4C3 hydrogel treated group was significantly higher than that in G8F4 hydrogel treated group and black group. For one thing, too fast degradation rate will lead to rapid failure of adhesion between hydrogel and corneal tissue. For another, the degradation rate of hydrogel should match the regeneration rate of corneal stroma, and too fast degradation will lead to thinner regenerated stroma. Similar findings have been reported. X. Shen prepared a hybrid hydrogel consisting of porcine decellularized corneal stroma matrix and methacrylated hyaluronic acid, exhibiting slow degradation, and enhanced mechanical properties & corneal adhesion. This hydrogel adhered intimately to the stroma bed with a long-term retention, which showed superior performance in accelerating corneal epithelial and stromal wound healing [36]. In the present study, G8F4 hydrogel showed faster degradation. If the degradation rate was too fast, the adhesion between G8F4 hydrogel and corneal tissue would be significantly reduced, which might lead to hydrogel shedding. The presence of COL I, specifically the cross-linked COL I in the hydrogel, delayed the degradation of hydrogel to ensure the adhesion between G8F4C3 hydrogel and corneal tissue. At the same time, the extended degradation duration matched the formation rate of the matrix and guaranteed more ideal corneal injury healing. Thus, the introduction of COL I not only promoted mechanical performance and adhesion ability of hydrogel, but also benefited corneal tissue regeneration.

Besides, histological examinations in Figs. 8B and 9C showed that there were epithelial cell layers in all three groups after 28 days post-implantation, while black group and G8F4 hydrogel treated group retained obvious defects with insufficient thickness. Masson trichrome staining revealed that the G8F4C3 hydrogel supported collagen fiber regeneration. Further IHC of α-SMA was carried out to identify corneal fibrosis. α-SMA expression in G8F4C3 hydrogel treated stroma was significantly lower than that in G8F4 hydrogel treated group, indicating that application of G8F4C3 hydrogel could reduce scar formation that could lead to irreversibly reduced transparency.

Taken together, the present G8F4C3 hydrogel patch assisted with CXL showed potential in the treatment of advanced corneal diseases such as severe keratoconus because it could fill and repair corneal defects, and reinforce the native cornea simultaneously.

At last, as reported in previous literature, a variety of sutureless corneal hydrogels have been developed to promote the regeneration of corneal epithelium and stroma, exhibiting excellent repair effects *in vivo*,

such as IonBAH, LC-COMatrix, LiQD Cornea [20,37,40,41]. Most of them were based on decellularized corneal matrix. Although G8F4C3 hydrogel in combination with CXL exhibited a wound-healing effect, it still failed to achieve perfect corneal regeneration compared to the above decellularized corneal matrix-derived hydrogels. Thus, bioactive factors and drugs can be added to the present "T.E.S.T" bioadhesive to inhibit the corneal fibrosis observed in the current study for further improvement.

4. Conclusion

In summary, F127DA and AF127 were synthesized for co-assembly to fabricate bi-functional micelles, which were introduced into GelMA to significantly improve the toughness of gelatin-based hydrogels after UV irradiation. The further addition of COL I could form a cross-linked network when combining CXL with the presence of RF, enhancing mechanical properties and cornea tissue adhesion performance. Based on the composition optimization, G8F4C3 hydrogel exhibited well-performed transparency, high toughness, and strong bio-adhesion. The precursor solution of G8F4C3 hydrogel injected into corneal defect could be gelled quickly and form stable integration with the native cornea, supporting re-epithelialization. During the 4 weeks *in vivo* assessments, the degradation of G8F4C3 hydrogel matched well with the rate of corneal stroma regeneration. Therefore, it was natural corneal tissue representativeness with a user-friendly application feature, possessing great potential for future ophthalmic surgeries.

Ethics approval

All experiments were conducted in compliance with the ARVO statement for the Use of Animals in Ophthalmology and Vision Research and had ethical approval from Animal Care Committees of Eye and ENT Hospital of Fudan University (IACUC-DWZX-2022-017).

CRediT authorship contribution statement

Meiyan Li: Conceptualization, Investigation, Methodology, Writing – original draft, preparation. **Ruoyan Wei:** Data curation, Investigation, Writing – original draft. **Chang Liu:** Investigation, Writing – review & editing. **Haowei Fang:** Methodology. **Weiming Yang:** Investigation. **Yunzhe Wang:** Investigation, Visualization. **Yiyong Xian:** Investigation. **Kunxi Zhang:** Conceptualization, Writing – original draft, preparation, Writing – review & editing, Supervision. **Yong He:** Writing – review & editing, Supervision. **Xingtao Zhou:** Project administration, Supervision, Funding acquisition.

Declaration of competing interest

The authors declare that they have no known competing financial interests or personal relationships that could have appeared to influence the work reported in this paper.

Acknowledgements

This work was supported by the Shanghai Rising-Star Program (Grants No. 21QA1401500), Clinical Research Plan of SHDC (Grants No. SHDC2020CR1043B).

Appendix A. Supplementary data

Supplementary data to this article can be found online at https://doi.org/10.1016/j.bioactmat.2023.02.006.

References

[1] J.H. Krachmer, R.S. Feder, M.W. Belin, Keratoconus and related noninflammatory corneal thinning disorders, Surv. Ophthalmol. 28 (1984) 293.
[2] P. Gain, R. Jullienne, Z. He, M. Aldossary, S. Acquart, F. Cognasse, G. Thuret, Global survey of corneal transplantation and eye banking, JAMA Ophthalmol 134 (2016) 167.
[3] B.H. Jeng, S. Ahmad, In pursuit of the elimination of corneal blindness: is establishing eye banks and training surgeons enough? Opthalmology 128 (2021) 813–815.
[4] M. Ahearne, J. Fernández-Pérez, S. Masterton, P.W. Madden, P. Bhattacharjee, Designing scaffolds for corneal regeneration, Adv. Funct. Mater. 30 (2020), 1908996.
[5] B. Kharod-Dholakia, J.B. Randleman, J.G. Bromley, R.D. Stulting, Prevention and treatment of corneal graft rejection current practice patterns of the cornea society, Cornea 34 (2015) (2011) 609–614.
[6] C.G. Christo, J. van Rooij, A.J. Geerards, L. Remeijer, W.H. Beekhuis, Suture-related complications following keratoplasty: a 5-year retrospective study, Cornea 20 (2001) 816–819.
[7] S. Matthyssen, B. Van den Bogerd, S.N. Dhubhghaill, C. Koppen, N. Zakaria, Corneal regeneration: a review of stromal replacements, Acta Biomater. 69 (2018) 31–41.
[8] R.N. Palchesko, S.D. Carrasquilla, A.W. Feinberg, Natural biomaterials for corneal tissue engineering, repair, and regeneration, Adv. Healthc. Mater. 7 (2018), 1701434.
[9] J.W. Ruberti, J.D. Zieske, Prelude to corneal tissue engineering—gaining control of collagen organization, Prog. Retin. Eye Res. 27 (2008) 549–577.
[10] R.R. Mohan, D. Kempuraj, S. D'Souza, A. Ghosh, Corneal stromal repair and regeneration, Prog. Retin. Eye Res. 91 (2022), 101090.
[11] M.W. Grinstaff, Designing hydrogel adhesives for corneal wound repair, Biomaterials 28 (2007) 5205–5214.
[12] P. Bhattacharjee, M. Ahearne, Significance of crosslinking approaches in the development of next generation hydrogels for corneal tissue engineering, Pharmaceutics 13 (2021) 319.
[13] S. Khosravimelal, M. Mobaraki, S. Eftekhari, M. Ahearne, A.M. Seifalian, M. Gholipourmalekabadi, Hydrogels as emerging materials for cornea wound healing, Small 17 (2021), 2006335.
[14] S. Sharif, M.M. Islam, H. Sharif, R. Islam, D. Koza, F. Reyes-Ortega, D. Alba-Molina, P.H. Nilsson, C.H. Dohlman, T.E. Mollnes, J. Chodosh, M. Gonzalez-Andrades, Tuning gelatin-based hydrogel towards bioadhesive ocular tissue engineering applications, Bioact. Mater. 6 (2021) 3947–3961.
[15] L. Li, C. Lu, L. Wang, M. Chen, J. White, X. Hao, K.M. McLean, H. Chen, T. C. Hughes, Gelatin-based photocurable hydrogels for corneal wound repair, ACS Appl. Mater. Interfaces 10 (2018) 13283–13292.
[16] G. Su, G. Li, W. Wang, L. Xu, Application prospect and preliminary exploration of GelMA in corneal stroma regeneration, Polymers 14 (2022) 4227.
[17] E.S. Sani, A. Kheirkhah, D. Rana, Z. Sun, W. Foulsham, A. Sheikhi, A. Khademhosseini, R. Dana, N. Annabi, Sutureless repair of corneal injuries using naturally derived bioadhesive hydrogels, Sci. Adv. 5 (2019), eaav1281.
[18] I.A. Khalil, B. Saleh, D.M. Ibrahim, C. Jumelle, A. Yung, R. Dana, N. Annabi, Ciprofloxacin-loaded bioadhesive hydrogels for ocular applications, Biomater. Sci. 8 (2020) 5196.
[19] X. Zhao, S. Li, X. Du, W. Li, Q. Wang, D. He, J. Yuan, Natural polymer-derived photocurable bioadhesive hydrogels for sutureless keratoplasty, Bioact. Mater. 8 (2022) 196–209.
[20] L. Zhao, Z. Shi, X. Sun, Y. Yu, X. Wang, H. Wang, T. Li, H. Zhang, X. Zhang, F. Wang, X. Qi, R. Cao, L. Xie, Q. Zhou, W. Shi, Natural dual-crosslinking bioadhesive hydrogel for corneal regeneration in large-size defects, Adv. Healthc. Mater. 11 (2022), 2201576.
[21] R. Tutar, E. Yüce-Erarslan, B. İzbudak, A. Bal-Öztürk, Photocurable silk fibroin-based tissue sealants with enhanced adhesive properties for the treatment of corneal perforations, J. Mater. Chem. B 10 (2022) 2912.
[22] A. Farasatkia, M. Kharaziha, Robust and double-layer micro-patterned bioadhesive based on silk nanofibril/GelMA-alginate for stroma tissue engineering, Int. J. Biol. Macromol. 183 (2021) 1013–1025.
[23] G.R.S. Franzco, Collagen cross-linking: a new treatment paradigm in corneal disease – a review, Clin. Exp. Ophthalmol. 38 (2010) 141.
[24] J.S. Stanojevic, J.B. Zvezdanovic, D.Z. Markovic, Riboflavin degradation in the presence of quercetin in methanol under continuous UV-B irradiation: the ESI–MS–UHPLC analysis, Monatsh. Chem. 146 (2015) 1787–1794.
[25] M. Yang, W. Xu, Z. Chen, M. Chen, X. Zhang, H. He, Y. Wu, X. Chen, T. Zhang, M. Yan, J. Bai, C. McAlinden, K.M. Meek, J. Yu, S. Ding, R. Gao, J. Huang, X. Zhou, Engineering hibiscus-Like riboflavin/ZIF-8 microsphere composites to enhance transepithelial corneal cross-Linking, Adv. Mater. 34 (2022), 2109865.
[26] M. Ahearnea, A. Coyle, Application of UVA-riboflavin crosslinking to enhance the mechanical properties of extracellular matrix derived hydrogels, J. Mech. Behav. Biomed. 54 (2016) 259–267.
[27] I.A. Barroso, K. Man, T.E. Robinson, S.C. Cox, A.K. Ghag, Photocurable GelMA adhesives for corneal perforations, Bioengineering 9 (2022) 53.
[28] R. Goto, E. Nishida, S. Kobayashi, M. Aino, T. Ohno, Y. Iwamura, Gelatin methacryloyl—riboflavin (GelMA—RF) hydrogels for bone regeneration, Int. J. Mol. Sci. 22 (2021) 1635.
[29] S. Kim, C.-C. Chu, Fabrication of a biodegradable polysaccharide hydrogel with Riboflavin, Vitamin B2, as a photo-initiator and L-Arginine as cointiator upon UV irradiation, J. Biomed. Mater. Res. B 91B (2009) 390–400.

[30] M.S.H. Akash, K. Rehman, Recent progress in biomedical applications of Pluronic (PF127): Pharmaceutical perspectives, J. Contr. Release 209 (2015) 120–138.
[31] R.N. Shamma, R.H. Sayed, H. Madry, N.S. El Sayed, M. Cucchiarini, Triblock copolymer bioinks in hydrogel three-dimensional printing for regenerative medicine: a focus on Pluronic F127, Tissue Eng. B Rev. 28 (2022) 451–463.
[32] X. Yu, Z. Qin, H. Wu, H. Lv, X. Yang, pH-driven preparation of small, non-aggregated micelles for ultra-stretchable and tough hydrogels, Chem. Eng. J. 342 (2018) 357–363.
[33] P. Sun, H. Zhang, D. Xu, Z. Wang, L. Wang, G. Gao, G. Hossain, J. Wu, R. Wang, J. Fu, Super tough bilayer actuators based on multi-responsive hydrogels crosslinked by functional triblock copolymer micelle macro-crosslinkers, J. Mater. Chem. B. 7 (2019) 2619.
[34] Z. Li, L. Liu, Y. Chen, Direct 3D printing of thermosensitive AOP127-oxidized dextran hydrogel with dual dynamic crosslinking and high toughness, Carbohydr. Polym. 291 (2022), 119616.
[35] X. Zhao, Multi-scale multi-mechanism design of tough hydrogels: building dissipation into stretchy networks, Soft Matter 10 (2014) 672–687.
[36] X. Shen, S. Li, X. Zhao, J. Han, J. Chen, Z. Rao, K. Zhang, D. Quan, J. Yuan, Y. Bai, Dual-crosslinked regenerative hydrogel for sutureless long-term repair of corneal defect, Bioact. Mater. 20 (2023) 434–448.
[37] G. Yazdanpanah, X. Shen, T. Nguyen, K.N. Anwar, O. Jeon, Y. Jiang, M. Pachenari, Y. Pan, T. Shokuhfar, M.I. Rosenblatt, E. Alsberg, A.R. Djalilian, A light-curable and tunable extracellular matrix hydrogel for in situ suture-free corneal repair, Adv. Funct. Mater. 32 (2022), 2113383.
[38] N. Oliva, J. Conde, K. Wang, N. Artzi, Designing hydrogels for on-demand therapy, Acc. Chem. Res. 50 (2017) 669–679.
[39] J. Chen, J. Yang, L. Wang, X. Zhang, B. Heng, D. Wang, Z. Ge, Modified hyaluronic acid hydrogels with chemical groups that facilitate adhesion to host tissues enhance cartilage regeneration, Bioact. Mater. 6 (2021) 1689–1698.
[40] C.D. McTiernan, F.C. Simpson, M. Haagdorens, C. Samarawickrama, D. Hunter, O. Buznyk, P. Fagerholm, M.K. Ljunggren, P. Lewis, I. Pintelon, D. Olsen, E. Edin, M. Groleau, B.D. Allan, M. Grifth, LiQD Cornea: pro-regeneration collagen mimetics as patches and alternatives to corneal transplantation, Sci. Adv. 6 (2020), eaba2187.
[41] F. Wang, W. Shi, H. Li, H. Wang, D. Sun, L. Zhao, L. Yang, T. Liu, Q. Zhou, L. Xie, Decellularized porcine cornea-derived hydrogels for the regeneration of epithelium and stroma in focal corneal defects, Ocul. Surf. 18 (2020) 748–760.